

Supporting Information for “Fano Resonance Enabled Infrared Nano-Imaging of Local Strain in Bilayer Graphene”

Jing Du(杜靖)^{1,2†}, Bosai Lyu(吕博赛)^{1,2†}, Wanfei Shan(单琬斐)^{1,2†}, Jiajun Chen(陈佳俊)^{1,2}, Xianliang Zhou(周先亮)^{1,2}, Jingxu Xie(谢京旭)³, Aolin Deng(邓奥林)^{1,2}, Cheng Hu(胡成)^{1,2}, Qi Liang(梁齐)^{1,2}, Guibai Xie(谢贵柏)⁴, Xiaojun Li(李小军)⁴, Weidong Luo(罗卫东)^{1,2,5*}, and Zhiwen Shi(史志文)^{1,2*}

¹Key Laboratory of Artificial Structures and Quantum Control (Ministry of Education), Shenyang National Laboratory for Materials Science, School of Physics and Astronomy, Shanghai Jiao Tong University, Shanghai, China.

²Collaborative Innovation Center of Advanced Microstructures, Nanjing, China.

³Institute of Physics, Xi’an Jiao Tong University, Xi’an, China.

⁴National Key Laboratory of Science and Technology on Space Science, China Academy of Space Technology (Xi’an), Xi’an, China.

⁵Institute of Natural Sciences, Shanghai Jiao Tong University, Shanghai, China.

†These authors contribute equally to this work.

*To whom correspondence should be addressed. Email: zwshi@sjtu.edu.cn, wdluo@sjtu.edu.cn

Section 1: Near-field IR nano-imaging of compressive strain in bilayer graphene

Section 2: Near-field IR nano-imaging of tensile strain in bilayer graphene

Section 3: Theoretical analysis of local strain near the end of a wrinkle

Section 1: Near-field IR nano-imaging of compressive strain in bilayer graphene

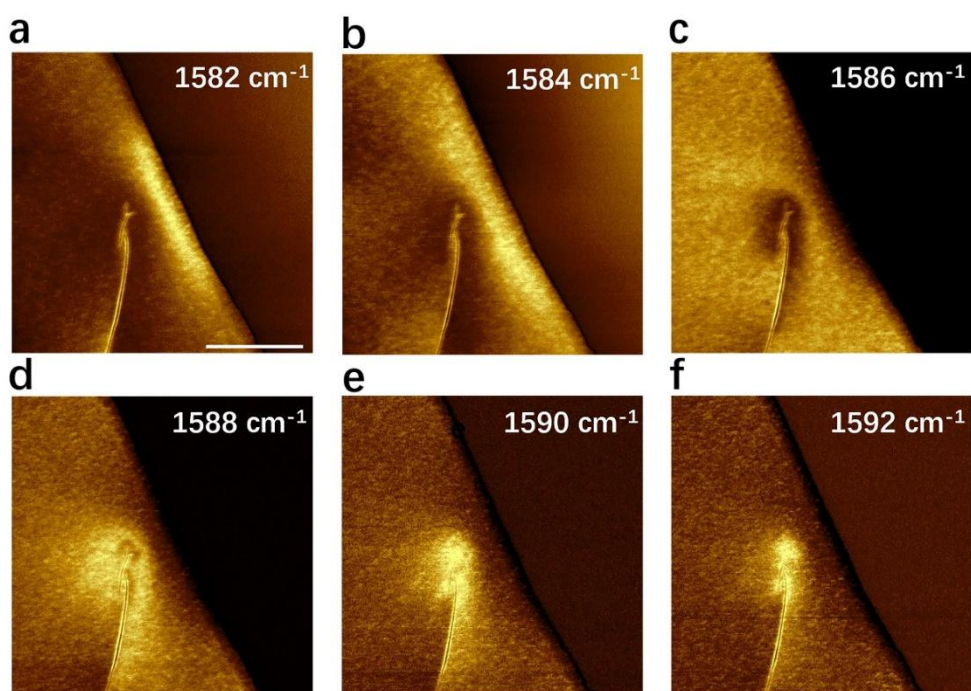


Figure S1. Additional s-SNOM images of compressive strain in bilayer graphene flakes with a wrinkle. In (a-c), at frequencies lower than intrinsic phonon frequency, near-field IR images feature a prominent dark spot near the end of wrinkle. In (d-f), at frequencies higher than phonon frequency, near-field IR images gradually become a bright spot at the strained areas. Scale bar 1 μm .

Section 2: Near-field IR nano-imaging of tensile strain in bilayer graphene

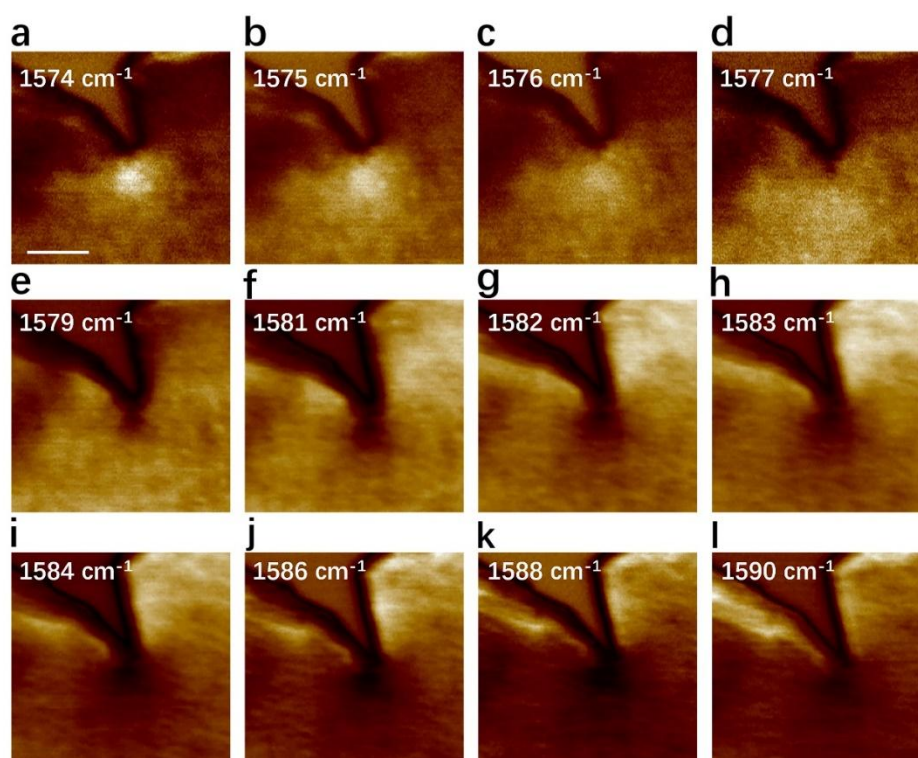


Figure S2. Additional s-SNOM images of tensile strain in bilayer graphene flakes with a crack. In (a-d), at frequencies lower than phonon frequency, near-field IR images feature a simply bright spot near the crack. In (e-l), at frequencies higher than phonon frequency, near-field IR images gradually become a dark spot at the strained areas. Scale bar 500 nm.

Section 3: Theoretical analysis of local strain near the end of a wrinkle

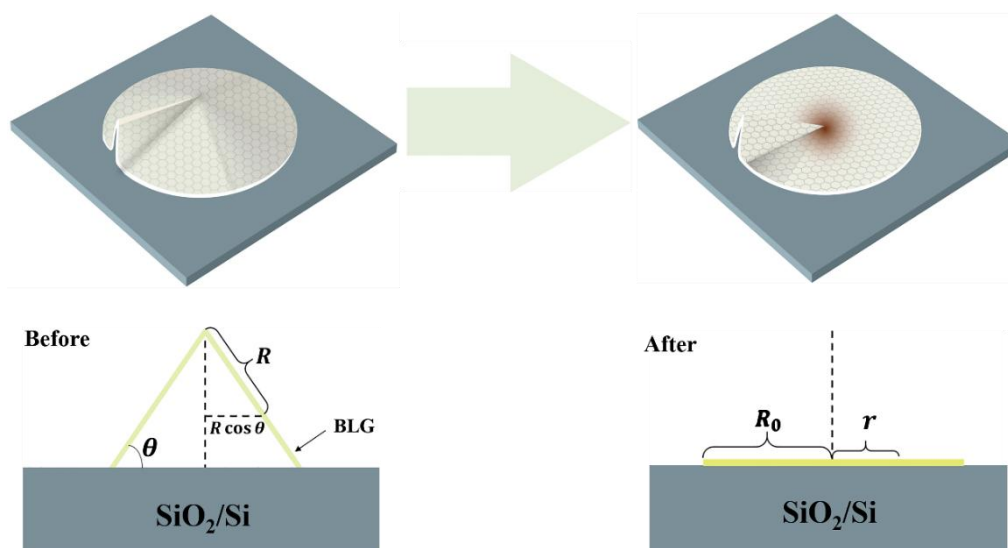


Figure S3. Bilayer graphene cone with a wrinkle before (left panel) and after (right panel) deformation.

In-plane strain exists near the end of wrinkles in a 2D membrane because of discontinuity of interior angle and can be understood by a process as showed in Figure S3. First, when the part of flat 2D membrane is folded to a wrinkle, a piece of the flat membrane is curved into a 3D cone and the corresponding central angle reduces to less than 2π . Second, if the 3D cone is compelling to a flat 2D membrane, the compressive strain will emerge. The distribution of the strain can be solved analytically.

In the polar coordinate system, the local strain near the end of the wrinkle satisfies the following conditions,

$$\frac{\partial \varepsilon_r}{\partial r} + \frac{\varepsilon_r - \varepsilon_\theta}{r} = 0, \quad (1)$$

$$\frac{\partial \varepsilon_r}{\partial \theta} = 0, \quad (2)$$

where ε_r and ε_θ are the radial and tangential strain, respectively. Here we have considered the rotational system and assumed that there is no shear strain in the model. Furthermore, we supposed that bilayer graphene flakes are isotropic and resiliency is in a linear region. The strain and the spatial deformation are described by the following formulas,

$$\varepsilon_r = \frac{dr}{dR} - 1, \quad (3)$$

$$\varepsilon_\theta = \frac{r}{R \cos \theta} - 1, \quad (4)$$

where θ is the angle between generatrix line and horizontal direction which is determined by the slope of wrinkle, R and r are the distance between a point on the cone to the apex before and after deformation, respectively. Plug Eq. (3) and Eq. (4) into Eq. (1), we can obtain,

$$\frac{d}{dr} \left(\frac{dr}{dR} \right) + \frac{1}{r} \left(\frac{dr}{dR} - \frac{r}{R \cos \theta} \right) = 0. \quad (5)$$

Here we think r as a function of R . By utilizing the substitution $d/dr = d/dR \cdot dR/dr$ and the Eq. (5) can be written as

$$\frac{d^2 r}{dR^2} + \frac{1}{r} \frac{dr}{dR} \left(\frac{dr}{dR} - \frac{r}{R \cos \theta} \right) = 0. \quad (6)$$

Considering the boundary conditions

$$\varepsilon_r|_{r=R_0} = 0, \quad (7)$$

$$r(0) = 0, \quad (8)$$

where R_0 is the radius of the deformed disk. With the boundary conditions, we can obtain a particular solution,

$$r = \left[\frac{(1-\gamma)R}{R_0^\gamma} \right]^{\frac{1}{1-\gamma}}, \quad (9)$$

where

$$\gamma = \frac{1-\cos \theta}{1+\cos \theta}. \quad (10)$$

Then Eq. (3) and Eq. (4) turn into

$$\varepsilon_r = \left(\frac{r}{R_0} \right)^\gamma - 1, \quad (11)$$

$$\varepsilon_\theta = (1-\gamma) \left(\frac{r}{R_0} \right)^\gamma - 1. \quad (12)$$

From the two functions, we can roughly estimate the strain amplitude by the topography of a wrinkle.